SCIENTIFIC REPORTS

OPEN

High-Speed Scalable Silicon-MoS$_2$ P-N Heterojunction Photodetectors

Veerendra Dhyani & Samaresh Das

Two-dimensional molybdenum disulfide (MoS$_2$) is a promising material for ultrasensitive photodetector owing to its favourable band gap and high absorption coefficient. However, their commercial applications are limited by the lack of high quality p-n junction and large wafer scale fabrication process. A high speed Si/MoS$_2$ p-n heterojunction photodetector with simple and CMOS compatible approach has been reported here. The large area MoS$_2$ thin film on silicon platform has been synthesized by sulfurization of RF-sputtered MoO$_3$ films. The fabricated molecular layers of MoS$_2$ on silicon offers high responsivity up to 8.75 A/W (at 580 nm and 3V bias) with ultra-fast response of 10 μsec (rise time). Transient measurements of Si/MoS$_2$ heterojunction under the modulated light reveal that the devices can function up to 50 kHz. The Si/MoS$_2$ heterojunction is found to be sensitive to broadband wavelengths ranging from visible to near-infrared light with maximum detectivity up to $\approx 1.4 \times 10^{12}$ Jones (2V bias). Reproducible low dark current and high responsivity from over 20 devices in the same wafer has been measured. Additionally, the MoS$_2$/Si photodetectors exhibit excellent stability in ambient atmosphere.

Transition metal dichalcogenides (TMDs) are predicted to be promising candidate for next generation electronics[1–3], optoelectronics[4,5], and sensor[6] devices. The intrinsic nature of carriers in two dimensional semiconductors offers numerous advantages such as high mobility, high sensitivity, fast response and chemical stability[7–10]. Among several of the layered TMDs, MoS$_2$ has attracted great interest because of its distinctive electronic, optical, and catalytic properties[4–6,9–12]. In the recent time a lot of efforts have been devoted to demonstrate the potential of MoS$_2$ for a variety of applications[13–15]. MoS$_2$ has been used as an active layer in high mobility transistors (70–100 cm^2/V-s) with very high on/off ratio of 10^8[16,17]. More importantly, the broad spectrum from which MoS$_2$ can absorb light i. e. visible to near-infrared spectral region (350–950 nm) is higher than GaAs and Si (one order of magnitude in a thickness of less than 1 nm) which makes it an ideal material for photonic devices[18,19]. However, the use of MoS$_2$ for practical applications is still limited due to the lack of scalability in its fabrication process. Several methods such as mechanical/chemical exfoliation, chemical vapour deposition etc[20–23]. that have been reported are mired with drawbacks. In the exfoliation method, poor control over thickness and limited size of MoS$_2$ films are the main deterrents. On the other hand there are reports available, where large-area MoS$_2$ layers has been directly obtained using chemical vapour deposition and solution processed methods[4,24,25]. The absence of high quality p–n junctions also limits the performance of the MoS$_2$ based devices. Although photodetectors based on mono/multilayer MoS$_2$ heterostructure have shown excellent device characteristics in terms of high sensitivity (up to 7 A/W) and wide band response[26–29] their applicability still suffers due to complex fabrication process.

In this work, we report Si/MoS$_2$ (p-n) heterojunction based photodetector contrived from a very simple, reproducible and scalable fabrication process. To fabricate the heterojunction, we have adopted CVD process for the growth of MoS$_2$ thin film as mentioned in previously published reports[24,26]. The durability and scalability of the devices examined after two months are found to remains intact. The fabricated heterojunction exhibited excellent photoresponse properties in the visible to near-infrared wavelengths with a maximum responsivity of 8.75 A W^{-1} and fast rise time of 10 μs. The excellent performance of multilayered MoS$_2$ heterostructure may lead the way for the fabrication of high speed photodetectors.

Experimental details

Synthesis of large area MoS$_2$ thin film.
In the present study, MoS$_2$ thin films were fabricated by the sulphurization of molybdenum trioxide (MoO$_3$) in N$_2$ ambient at low temperature. In a typical process, a 10 nm thick film of MoO$_3$ was first deposited on the SiO$_2$/Si substrates by reactive sputtering (in presence of Ar and O$_2$

Centre for Applied Research in Electronics, Indian Institute of Technology Delhi, New Delhi-110016, India. Correspondence and requests for materials should be addressed to S.D. (email: samareshdas@care.iitd.ac.in)
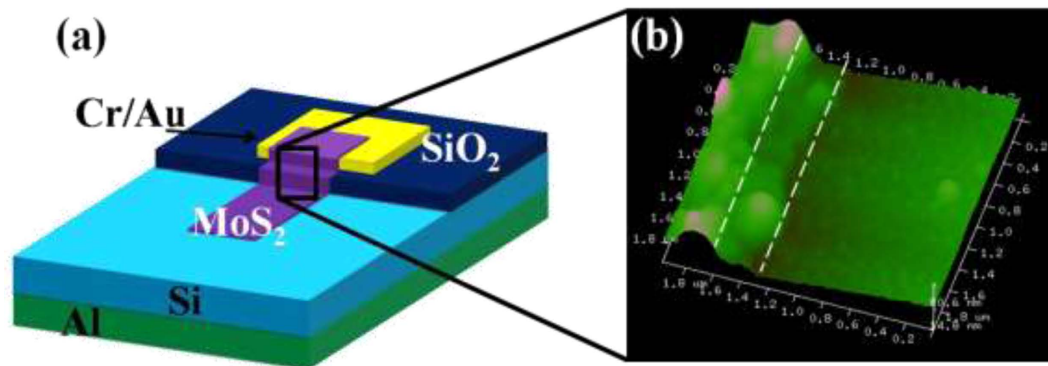
Figure 1. Schematic representations of the Si/MoS$_2$ p-n heterojunction photodetector, (**b**) AFM image of MoS$_2$ layer at metal contact and heterojunction interface.
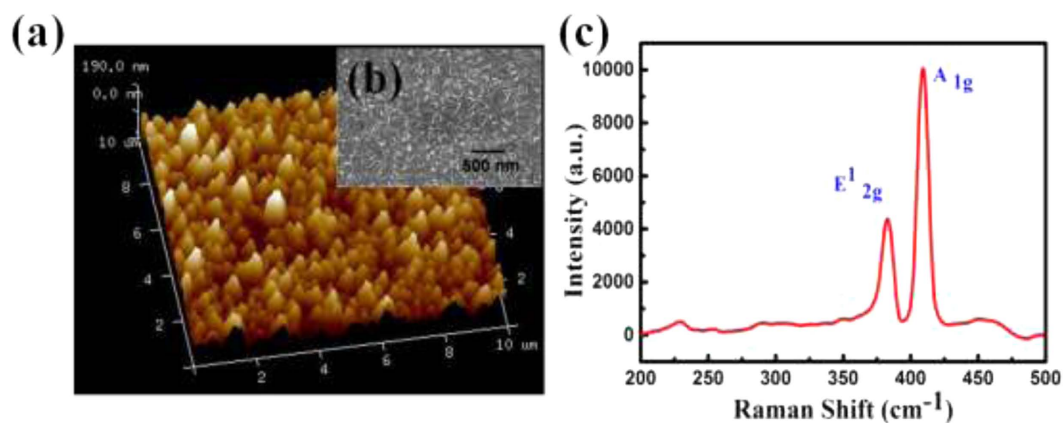

Figure 2. (**a**) AFM image and (**b**) Raman spectra of as synthesized MoS$_2$.

with 1:1 ratio). The MoO$_3$/SiO$_2$/Si samples were then placed at the centre of a tube furnace preheated to 500 °C and maintained for 20 min. Sulphur powder was introduced in the upstream zone of the furnace, where temperature is around 200 °C. As a result of the sulphurization process, thin films of MoS$_2$ with large area coverage were grown. The structural and morphological properties of deposited samples were characterized by Scanning electron microscopy (SEM- Ziess evo 18), and atomic force microscopy (AFM- Bruker dimension). In order to confirm the formation of MoS$_2$ Raman spectroscopy (Horiba Raman Lab RAM HR 800 Evolution) has been employed.

Device fabrication and measurements. Si/MoS$_2$ heterojunction photodetectors were fabricated using C-MOS compatible technology. P-type silicon (100) with a thermally grown silicon oxide (SiO$_2$) of 100 nm was used as the starting wafer for the fabrication of Si/MoS$_2$ heterojunction. To expose the silicon, SiO$_2$ was selectively etched after the first UV-lithography step. A two step photo-lithography process has been used to make the heterojunction. In the first step, squares of dimension 100 μm^2 were opened in SiO$_2$, which define the Si/MoS$_2$ junction area. The metal contact (Cr/Au) has been patterned in the second lithography process. The detailed fabrication process is given in the supplementary information (Fig. S1). On the top of this structure, thin layer of MoO$_3$ (10 nm) was deposited by reactive sputtering. Samples were cleaned in the oxygen plasma for 30 sec before the deposition of MoO$_3$. After the deposition of MoO$_3$, MoS$_2$ was grown via sulphurization process discussed earlier. Cr/Au layers on the top serve as the one electrode for the electrical measurements, while a 100 nm thick layer of Al has been deposited on the back side of the silicon for second electrode. Figure 1(a) shows a typical schematic representation of the device structure. MoS$_2$ thin film on Si and metal contact can be seen in the AFM image Fig. 1(b). In order to measure the photoresponse of Au-MoS$_2$-Au metal-semiconductor-metal (MSM) photodetector was fabricated. The fabrication process was the same as Si/MoS$_2$ heterojunction, except that the bottom oxide was not etched. Electrical measurements of the device were performed using Keithley semiconductor analyzer (SCS4200) under ambient conditions. The spectral response of the photodetector has been measured in the wavelength range 300 nm to 1100 nm.

Results and Discussion

The morphology of the as deposited MoS$_2$ film surface observed under an atomic force microscopy (AFM) is shown in Fig. 2(a). The surface of the film seems to be composed of vertically aligned nanoflakes with average
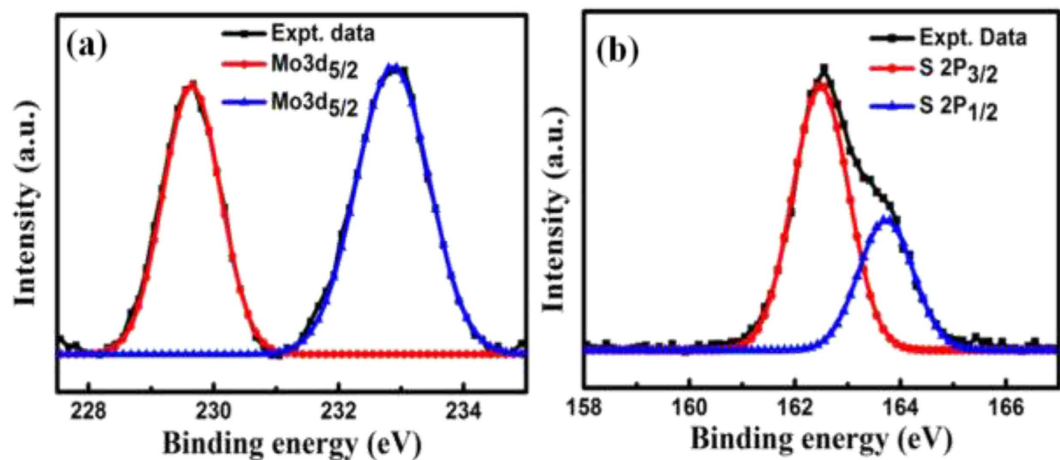
Figure 3. (**a**) and XPS spectra showing the binding energy of (**a**) Mo 3d and (**b**) S 2p electron.

width between 20–40 nm. It is likely that these stratified features in the MoS$_2$ thin film formed as a result of the difference in the thermal expansion coefficient of substrate and the MoS$_2$ film during sulfurization. The growth of MoS$_2$ film was homogenous and it covered the entire substrate surface (~2inch) uniformly. Similar growth has been observed by Ellmer et al.[30] and S. B, Sadale et al.[31] in case of WS$_2$. A Scanning electron microscope (SEM) image of the as synthesized MoS$_2$ is shown in the inset of Fig. 2(a). The above SEM image confirms clearly the formation of nanoflakes of MoS$_2$. Similar morphology of MoS$_2$ surfaces has also been observed on SiO$_2$ substrate (Fig. S2(b) supplementary information). It is believed that this morphology originates from the hexagonal basal plane symmetry of the MoS$_2$ crystal itself, suggesting that the layers grown are oriented along c-axis of the MoS$_2$ unit cell[24,32]. A crystallinity of the MoS$_2$ thin film samples were examined using Raman spectroscopy (514 nm laser and 10 mW power). The characteristic Raman peaks for the E$^1_{2g}$ and A$_{1g}$ vibration modes appeared at 384 cm^{-1} and 408 cm^{-1} corresponding to MoS$_2$ hexagonal phase, as shown in Fig. 2(c)[24,32]. The overall intensity of the peaks and the relative ratio, of the E^1 2 g, the A$_{1g}$ peaks were similar to that from high quality exfoliated MoS$_2$. The crystallinity of the MoS$_2$ thin film was further investigated by XRD spectra (shown in Fig. S2(c) supplementary information). The preferred direction of growth was found to be along the c-axis (0001) of hexagonal phase[24,32,33]. This suggests that these films were of good structural quality.

The chemical bonding and electronic properties of the MoS$_2$ films were investigated by X-ray photoelectron spectroscopy (XPS) using Al–K$_\alpha$ radiation of energy 1486.6 eV. Binding energies of Mo 3d and S 2p electrons are shown in Fig. 3(a,b). Two distinct peaks for Mo 3d electrons observed at 229.4 and 232.6 eV were attributed to 3d$_{5/2}$ and 3d$_{3/2}$ chemical states, respectively[34–38]. The possibility of Mo-silicide or migration of Mo in Si was investigated by comparing the XPS peaks of Mo and Si with that reported in literature. The silicide related peaks of Mo are reported at lower binding energies for 3d$_{5/2}$ and 3d$_{3/2}$[35,36]. Similarly the XPS peak of Si 2P$_{3/2}$ was observed at 99.4 eV, which gets shifted towards lower binding energy for the Mo-silicide formation. In our samples the peak position of Si 2P$_{3/2}$ has been observed at 102.3 eV[35,36] (Fig. S2(a) in supplementary information). XPS analysis for both of the Mo and Si clearly confirmed that formation of silicide or migration of Mo in Si has not occurred in our samples. The spectrum for S 2p electrons is resolved into Gaussian peaks located at 162.5 eV and 163.8 eV, owing to S 2p$_{3/2}$ and S 2p$_{1/2}$ states, respectively. The observed peak positions of spin-orbit coupled Mo 3d and S 2p electrons are in excellent agreement with those reported in literature[33], confirming the synthesis of pure hexagonal 2-H phase MoS$_2$.

In general bulk MoS$_2$ exhibit n-type conductivity and makes a type –II p-n junction with the p-Si. Since the Raman spectra from the as-synthesized MoS$_2$ sample shows a splitting of more than 25 cm^{-1} between E$^1_{2g}$ (384 cm^{-1}) and A$_{1g}$ (408 cm^{-1}) modes, which is similar to bulk (multilayered) structure[34,36–39]. A typical current-voltage (I–V) characteristic of the Si/MoS$_2$ heterojunction under the light and dark condition is depicted in Fig. 4(a). During the measurement, the p-type substrate was kept at ground and the bias voltage was applied to the top MoS$_2$ contact and therefore a negative voltage to the top contact would make the junction forward biased. The voltage biasing scheme is shown in the inset of Fig. 4(a). The high asymmetry observed in the I–V characteristics clearly indicates the formation of a very good p-n junction between the n-type MoS$_2$ and p-type Si. A dark current of ~1.8 × 10^{-7}was measured at reverse bias of 3 V, which enhances ~127 times upon illumination under 560 nm light of intensity 5 mW/cm^2. In order to estimate the ideality factor η of the fabricated heterojunction, the semi-log J-V plot has been fitted according to the following equation[18,34].

$$\eta = \frac{q}{k_B T}\frac{dV}{dlnJ}$$

(1)

Here q is the unit charge, k$_B$ is the Boltzmann's constant, and J is current density. Current density (J) versus voltage (V) plot of the n-MoS$_2$ and p-Si heterojunction is given in the supplementary information (Fig. S3(a)). The diode ideality factor is found to be ~2.4. Since no passivation layer exists at the MoS$_2$-Si interface, the relatively large ideality factor might have originated due to the existence of interface defects states[34]. Furthermore, the
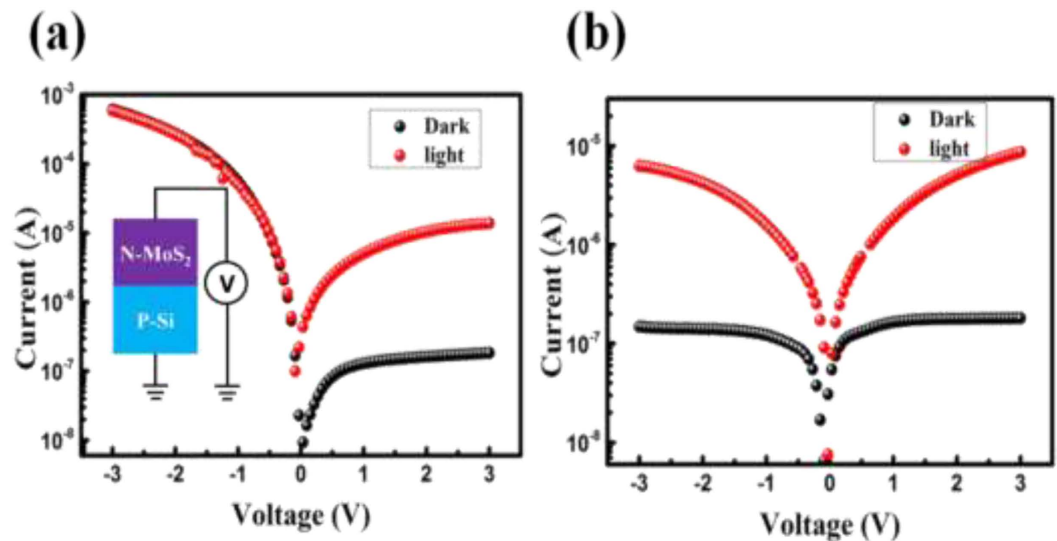
Figure 4. I-V characteristics of (**a**) Si-MoS$_2$ p-n heterojunction and (**b**) Au/MoS$_2$/Au MSM photodetector.

I-V curve of the heterojunction in the dark could be described by thermionic emission theory of charge carriers over a potential zero bias barrier Φ_b, from the Si to MoS$_2$. Φ_b can be defined by the following equation[18].

$$\Phi_b = \frac{k_B T}{q} \ln\left(\frac{AA^* T^2}{I_s}\right)$$

(2)

Here A is the area ($100 \times 100 \,\mu\text{m}^2$) of the device, A* ($32 \,\text{A cm}^{-2}\text{K}^{-2}$ for p-Si) is the effective Richardson constant. Based on the above equations, Φ_b was estimated to be approx. 0.545 eV. The C–V measurement on this heterojunction has been carried out and has been added as Fig. S3(b) in supplementary information. The used p-silicon wafers were boron doped with $\sim 10^{15}\,\text{cm}^{-3}$. From the C–V analysis the doping concentration for MoS$_2$ of $\sim 2 \times 10^{16}\,\text{cm}^{-3}$ was extracted for C-V analysis. Photoresponse of MoS$_2$ MSM photodetector was measured under the same illumination level to compare the performance with the MoS$_2$-Si p-n junction. Figure 4(b) shows the IV characteristics of Au- MoS$_2$-Au MSM photodetector. The measured dark current for MSM photodetector was found to be $\sim 2.5 \times 10^{-7}$ (at reverse bias of 3 V). Upon illumination (560 nm) a photo-to-dark current ratio of ~ 72 is achieved. For a better comparison MSM photodetector with one side Au and one side ohmic (low work function metal Ag) contact was made. I-V characteristic of Au-MoS$_2$-Ag is shown in Fig. S4(a). Semi ohmic nature (low rectification ratio of ~ 4) indicates the low barrier height of Au-MoS$_2$ contact[39]. Additionally the photocurrent the two MSM photodetectors are not much different from each other (Fig. (S4(b)). From these results it can be easily noted that the MoS$_2$-Si heterojunction possess larger gain than the MoS$_2$ MSM photodetector. The high rectification ratio, low turn-on voltage, and small ideality factor coupled with high photoresponse clearly demonstrate the high quality of the fabricated heterojunction photodetector.

The conduction mechanisms behind the operation of Si/MoS$_2$ heterojunction photodetectors can be explained using the help of energy band diagrams, as shown in Fig. 5. The alignment of the conduction and valence band edges of Si and MoS$_2$ in proper energy scale, is shown in Fig. 5(a). Under an equilibrium condition (zero bias), the band diagram of the MoS$_2$-Si heterojunction would be as shown in Fig. 5(b), where an electron affinity of 4.3 and a band gap of 1.8 for MoS$_2$ was assumed[34,40]. Since the thickness of MoS$_2$ layer is around 4–6 nmit would be fully depleted. As a result no bend bending in the energy band diagram in MoS$_2$ is expected as shown in Fig. 5(b). When the junction is formed between p-type Si with a work function (Φ Si) of 4.9 eV and n-type MoS$_2$ (Φ MoS$_2$ ~ 4.7 eV)[34], a large barrier potential would be created at the MoS$_2$/Si interface. On applying a reverse bias, the E_f (p-Si) is lifted to higher values, as shown in Fig. 5(c). That in turn enhances the electric field across the depletion region gradually and results in the expansion of barrier potential as well. This will open up a large number of accessible states for the holes to be injected into Si region. Here the higher carrier mobility of MoS$_2$ also helped to enhance the photoresponse of the photodetector. Under light illumination, electron–hole pairs are generated, which are then separated by this large barrier potential and collected by the electrodes. As a result of that photocurrent, which was totally suppressed near $V \approx 0$, significantly improves under small reverse bias.

Next, the photoresponse from Si/MoS$_2$ heterojunction and MoS$_2$ MSM devices were measured within the wavelength range 350 nm to 1050 nm. Spectral responsivity of a photodetector is directly proportional to the internal gain and it represents the efficiency of a detector for the specific optical signals. Responsivity of a photodetector can be defined as follows[40–43].

$$R(\lambda) = \left(\frac{I_{ph}}{P_{in}(\lambda)}\right) = \left(\frac{I_L - I_d}{P_{in}(\lambda)}\right)$$
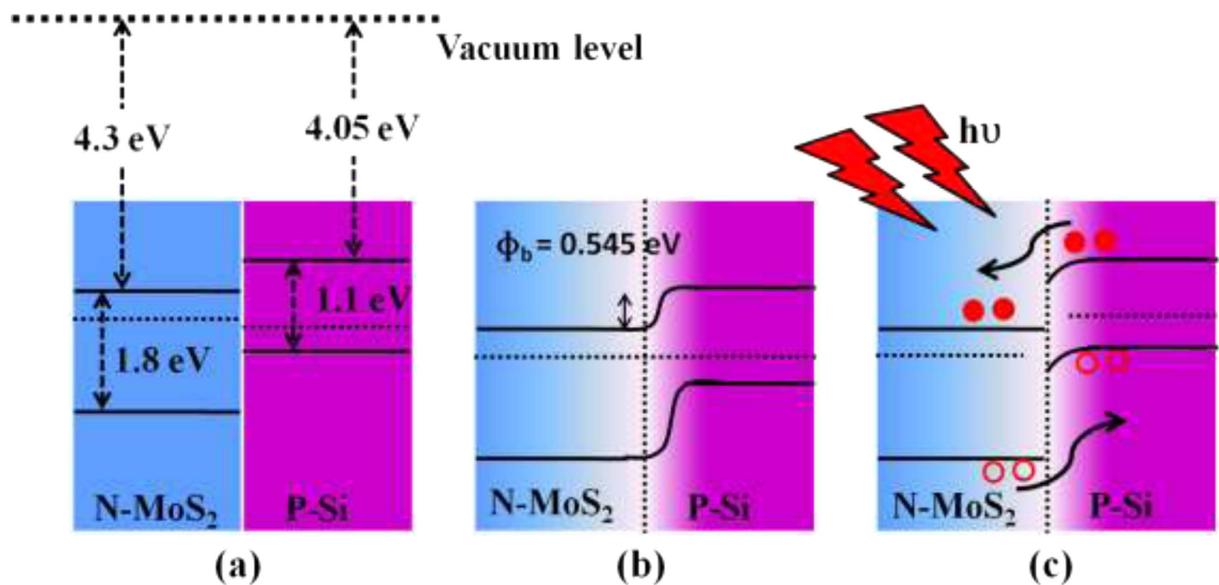
(3)

Figure 5. (**a**) Band edge alignment of Si/MoS$_2$ heterostructure and band diagram of MoS$_2$-Si heterojunction (**b**) at 0 V bias (**c**) at reverse bias.
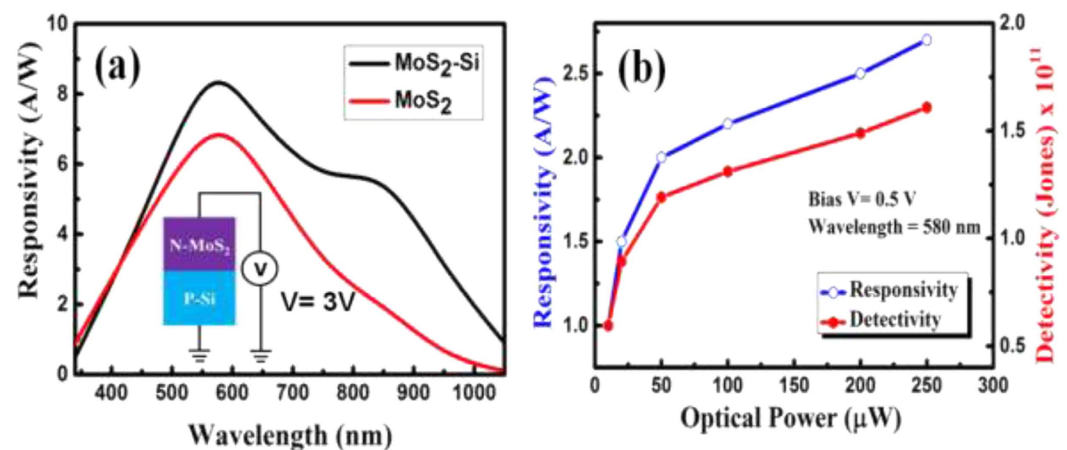

Figure 6. (**a**) responsivity of Si/MoS$_2$ heterojunction and MoS$_2$ MSM photodetector (inste shows the biasing condition for Si/MoS$_2$ heterojunction) and (**b**) optical power density dependent responsivity and detectivity of Si/MoS$_2$ heterojunction photodetector.

Here I_L and I_d are the current under light and dark condition, while P_{in} is the incident optical power density. Figure 6(a) shows the spectral response from the MoS$_2$/Si heterojunction and MoS$_2$ MSM device at a bias of 3 V. Boththe devices register a wide spectral response, for wavelength ranging from 450 nm–1000 nm. Two prominent peaks centered around 580 nm and 860 nm were observed for Si/MoS$_2$ heterojunction. On the other hand, for MoS$_2$ MSM photodetector, a single the peak was observed at 580 nm. It can therefore be concluded that the high responsivity at 580 nm is due to the absorption of MoS$_2$ film in the visible region[34]. The other peak at a wavelength of 860 nm corresponds to conventional Si based photodiode, which was observed from the absorption of the Si substrate[42]. As can be seen from Fig. 6(a), the responsivity for the MoS$_2$ MSM photodetector in the longer wavelength range (greater than 600 nm) is relatively lower than Si/MoS$_2$ heterojunction, due to the absence of Si junction. The improved photoresponse from MoS$_2$-Si device can be explained as follows. The introduction of the p-n heterojunction in the MoS$_2$/Si photodetector leads to the formation of an inherent large barrier height (depletion region) which gets further enhanced under a reverse bias. Under light illumination, electron–hole pairs are generated, which then gets separated by the large electric field and are collected at electrodes. The performance MoS$_2$/Si heterojunction photodetector also has contribution from the surface morphologies of deposited MoS$_2$ film. The photo-carrier generation and collection efficiency might have been enhanced due light trapping phenomena and high photosensitivity from the textured feature (nanostructures) at the surface. The high mobility of carrier in MoS$_2$-Si p-n junction due to high electric field might be another of the contributing factor. The value of responsivity for MoS$_2$-Si and MoS$_2$ MSM photodetector as shown in Fig. 6(a) measured at 580 nm are 8.50 A/W

and 6.8 A/W respectively. It is known that high reflection losses reduces the responsivity at smaller wavelengths, while for the longer wavelengths, reduction in responsivity is caused by band gap limit. Apart from responsivity (R), the performance of any photodetector can be expressed by detectivity (D*). These two characteristics properties are related to each other according to following equation[4,18,34].

$$D* = \frac{A^{1/2}R}{(2qI_d)^{1/2}}$$

(4)

Detectivity represents the ability of a detector to detect weak optical signals, which has been calculated from the above equation. It is assumed that the dark current is dominated by the shot noise for estimating detectivity. The other sources of noise (Johnson and flicker noise) are mainly thermal fluctuations, which can be neglected. Equation (4) suggests that a low dark current and a high responsivity are desired for the photodetector to exhibit high detectivity. The peak detectivity of the fabricated p-n heterojunction diode is estimated to be $\sim 2 \times 10^{11}$ cm-Hz$^{1/2}$. W^{-1} (or Jones) at 0.5 V bias, which get enhanced up to $\sim 1.4 \times 10^{12}$ Jones for 2 V bias. High detectivity indicates that the MoS$_2$-Si heterojunction is extremely sensitive to small optical input signals. The order of detectivity found in this work is high compare to other reported MoS$_2$-based photodetectors[4,7,18,34]. Most importantly, the high D* is acquired at small external bias voltage (0.5 V), in contrast to the relatively high bias voltage needed in previous works[4,18,34]. Figure 6(b) shows the linear increase of both responsivity and detectivity for low power illumination, and a a sub-linear dependence at higher power levels. The increase of illumination intensity leads to the enhanced electron–hole pair generation rate, resulting in a higher photocurrent. Under weak light intensity, the photogenerated electrons in MoS$_2$ will be captured by the trap states. As a result of reduced recombination, the lifetime for the photogenerated holes can be greatly prolonged, leading to higher R and D*. However, the available states will be remarkably reduced with increasing light intensity, eventually causing the saturation of photoresponse[34]. The sub-linear behaviour of the responsivity and detectivity (Fig. 6(b)) indicates that trap states in the MoS$_2$ layer or at the junction interface is responsible for this phenomenon.

Transient measurements of Si/MoS$_2$ junction under different illumination level are shown in Fig. S4 (supplementary information). The steep rise and fall edges suggest a fast response speed, indicating that electron–hole pairs could be effectively generated and separated in the Si/MoS$_2$ heterojunction. To further investigate the response time of MoS$_2$-Si heterojunction, transient measurements were performed under the illumination of modulating light source. A modulated laser source of wavelength 660 nm was used for these experiments. Response of the fabricated devices has been extracted in terms of the voltage across a resistance of 100 KΩ connected to the device (in series). The schematic representations of measurement setup and time response characteristics (for 10 kHz modulation) are given in the supplementary information (Fig. S4). The measurements have been carried out with a modulation up to 50 kHz of laser source. Figure 7(a) shows the time response of Si/MoS$_2$ photodetector under the 1 kHz modulated light. In the time domain, the speed of a PD is often characterized by the rise time (τ_r, the time interval from10% to 90% of the maximum photocurrent) and the fall time (τ_f, the time interval from 90% to 10% of the maximum photocurrent) of its response to an impulse signal. The magnified plot of time response for one cycle is shown in Fig. 7(b). Further analysis reveals a small τ_r of 10 µs, as well as a small τ_f of 19 µs. The values obtained here are remarkably high and much faster than any other reported MoS$_2$-based PDs Time response of the Si/MoS$_2$ heterojunction for 50 kHz laser modulation is also shown inset of Fig. 7(c). The high performance of the photodetector could be ascribed to the following aspects. First, the existence of a strong build-in electric field at the MoS$_2$ and Si interface can greatly facilitate the separation and transport of photo-generated carriers. This leads to the large response and relatively high speed of the heterojunction. Second aspects is the high in-plane mobility of carriers in the MoS$_2$ layer, which offers high speed paths for the transport of photogenerated carriers in this vertically standing layered structure. For 100 K ohm load resistance the cut off frequency obtained from the following eq. (5) should be 33.3 kHz.

$$f = \frac{1}{2\pi RC}$$

(5)

This high cut off frequency reflects in the high speed operation of the present device. The relative change in the current ($I_{ph(\upsilon)}$) of the photocurrent as a function of frequency in the range from 10 to 500 kHz is shown in Fig. 7(d). The relative change (defined as $I_{ph(\upsilon)} = I_L - I_d$)of the photocurrent only decreases by 50% at a high frequency of $\approx$40 kHz, implying that the Si/MoS$_2$ based PDs can operate at much higher frequencies. A comparison of improved performances of our Si/MoS$_2$ heterostructure has been given in Table 1 with other MoS$_2$ based photodetectors.

The scalability of the process has also been investigated. Twenty devices has been fabricated and tested on the same substrate. The responsivity and dark current variation of these devices are shown in Fig. 8(a). A negligible differences in the responsivity and dark current shows the reproducibility of the measurements, which reflects in the high scalability of the fabrication process. Similarly the scalability of Au-MoS$_2$-Au MSM photodetector was also investigated. The responsivity and dark current measurements for the 20 devices fabricated on the same substrate are presented in supplementary information. Furthermore, we investigated the air stability of the Si/MoS$_2$ photodetector by exposing it directly in air for more than three months without any encapsulation and found the similar results. Figure 8(b) shows I-V characteristics of Si/MoS$_2$ under normal ambient conditions. The device has been tested for consecutive three months and shows good atmospheric stability.

Conclusion

Si/MoS$_2$ heterojunction was fabricated by depositing MoS$_2$ films with a vertically standing layered structure on p-type silicon. MoS$_2$ layer was grown on wafer scale using the sulphurization MoO$_3$ thin films. The devices exhibit
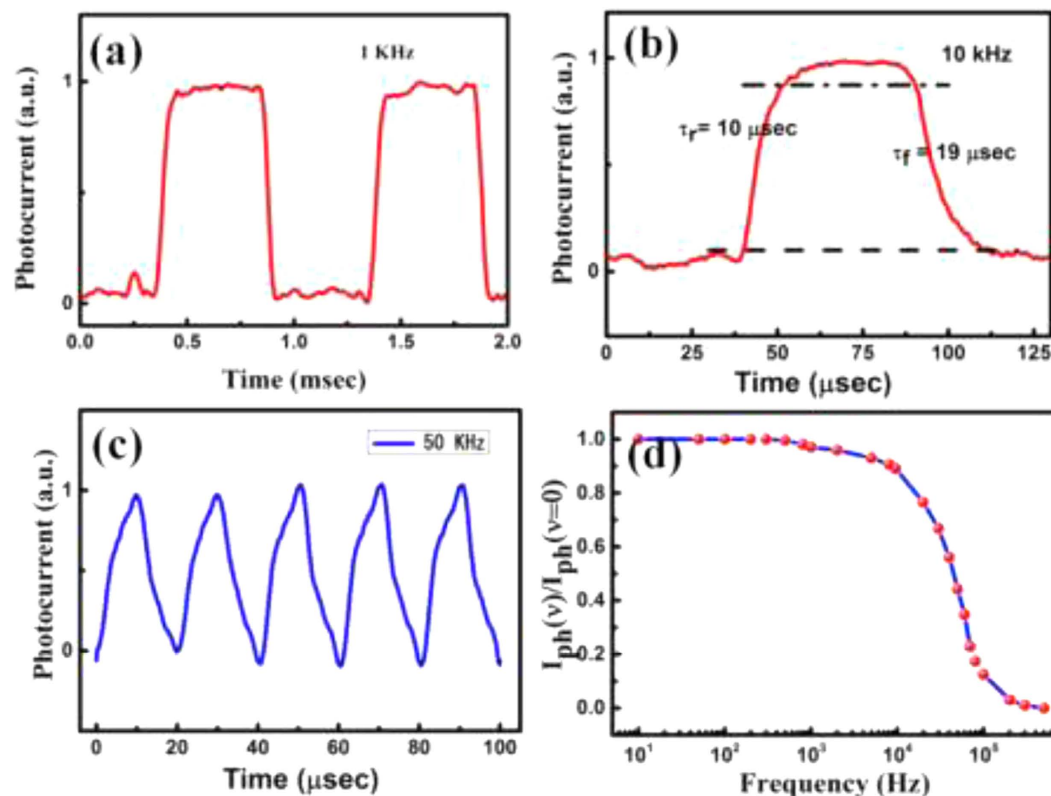
Figure 7. Time response characteristics under modulated light (**a**) 1 kHz, (**b**) 10 kHz (magnified), (**c**) 50 kHz and (**d**) Frequency dependence of normalized relative change in photocurrent (Iph(υ)/Iph(0)).
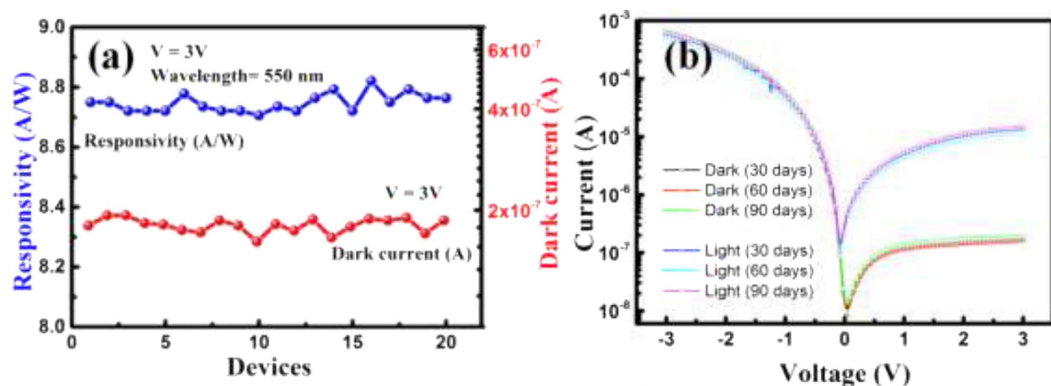

Figure 8. Scalability and stability test. (**a**) responsivity and dark current of 20 devices fabricated in simultaneously on single substrate, (**b**) I-V characteristics of Si/MoS$_2$ photodetector for different time period.

PDs structure (Device area)	Responsivity (A/W)	Response time($\tau r/\tau f$)	Detectivity (Jones)	Ref.
MoS$_2$ Schottky MSM PDs	1.04 A W^{-1}	40/50 μs		22
Si/MoS$_2$ heterojunction	7	50/50 ms	10^{10}	29
MoS$_2$-QD/Si heterostructure	2.8	-	0.8×10^{12}	34
Si/MoS$_2$ heterojunction (5 × 5 μm^2)	11.9	30.5/71.6 μs	—	4
MoS$_2$ Schottky MSM PDs	0.55- 1	0.2/1.7 ms	—	13
Si/MoS$_2$ heterojunction (10 × 10 μm^2)	0.210	0.3/0.3 ms	—	40
Si/MoS$_2$ heterojunction	8.75 A/W	10/19 μs	1.4×10^{12}	This Work

Table 1. A Comparison of the performance of MoS$_2$ and heterojunction based photodetector.

excellent photosensitive characteristics such as large responsivity (~8.75 A/W for 580 nm at 3 V bias), high detectivity (~1.4×10^{12} Jones for 2 V bias) and very fast time response of 10 μsec. Transient measurements reveal that our photodetector exhibits excellent stable and reproducible dynamic response upon high frequency pulsed light, enabling it suitable for high-frequency or high-speed optical- switch applications. Moreover, the combination of reproducible and scalable fabrication process used in this work should be suitable for multiplexed photodetector arrays.

References

1. Ganatra, R. & Zhang, Q. Few-Layer MoS₂: A Promising Layered Semiconductor. *Acs Nano* **8,** 4074–4099 (2014).
2. Mak, K. F., Lee, C., Hone, J., Shan, J. & Heinz, T. F. Atomically Thin MoS₂: A New Direct-Gap Semiconductor. *Phys. Rev. Lett.* **105,** 136805 (2010).
3. Gupta, A., Sakthivel, T. & Seal, S. Recent development in 2D materials beyond graphene. *Prog. Mater. Sci.* **73,** 44–126 (2015).
4. Zhang, Y. *et al. In Situ* Fabrication of Vertical Multilayered MoS₂/Si Homotype Heterojunction for High-Speed Visible-Near-Infrared Photodetectors. *Small Weinh. Bergstr. Ger.* **12,** 1062–1071 (2016).
5. Mak, K. F. & Shan, J. Photonics and optoelectronics of 2D semiconductor transition metal dichalcogenides. *Nat. Photonics* **10,** 216–226 (2016).
6. Cho, B. *et al.* Charge-transfer-based Gas Sensing Using Atomic-layer MoS₂. *Sci. Reports* **5,** 8052 (2015).
7. Li, X. *et al.* High Detectivity Graphene-Silicon Heterojunction Photodetector. *Small* **12,** 595–601 (2016).
8. Bhimanapati, G. R. *et al.* Recent Advances in Two-Dimensional Materials beyond Graphene. *Acs Nano* **9,** 11509–11539 (2015).
9. Riazimehr, S. *et al.* Spectral Sensitivity of Graphene/Silicon Heterojunction Photodetectors. *Solid-State Electron.* **115,** 207–212 (2016).
10. Butler, S. Z. *et al.* Progress, Challenges, and Opportunities in Two-Dimensional Materials Beyond Graphene. *Acs Nano* **7,** 2898–2926 (2013).
11. Dolui, K., Rungger, I. & Sanvito, S. Origin of the n-type and p-type conductivity of MoS₂ monolayers on a SiO₂ substrate. *Phys. Rev. B* **87,** 165402 (2013).
12. Li, H. *et al.* Optical Identification of Single- and Few-Layer MoS₂ Sheets. *Small* **8,** 682–686 (2012).
13. Lu, J. *et al.* Improved Photoelectrical Properties of MoS₂ Films after Laser Micromachining. *Acs Nano* **8,** 6334–6343 (2014).
14. Zu, S. *et al.* Active Control of Plasmon–Exciton Coupling in MoS₂–Ag Hybrid Nanostructures. *Adv. Opt. Mater.* doi: 10.1002/adom.201600188 (2016).
15. Lopez-Sanchez, O., Lembke, D., Kayci, M., Radenovic, A. & Kis, A. Ultrasensitive photodetectors based on monolayer MoS₂. *Nat. Nanotechnol.* **8,** 497–501 (2013).
16. Wang, H. *et al.* Integrated Circuits Based on Bilayer MoS₂ Transistors. *Nano Lett.* **12,** 4674–4680 (2012).
17. Nourbakhsh, A., Zubair, A., Dresselhaus, M. S. & Palacios, T. Transport Properties of a MoS₂/WSe₂ Heterojunction Transistor and Its Potential for Application. *Nano Lett.* **16,** 1359–1366 (2016).
18. Wang, L. *et al.* MoS₂/Si Heterojunction with Vertically Standing Layered Structure for Ultrafast, High-Detectivity, Self-Driven Visible–Near Infrared Photodetectors. *Adv. Funct. Mater.* **25,** 2910–2919 (2015).
19. Bernardi, M., Palummo, M. & Grossman, J. C. Extraordinary sunlight absorption and one nanometer thick photovoltaics using two-dimensional monolayer materials. *Nano Lett.* **13,** 3664–3670 (2013).
20. Li, H., Wu, J., Yin, Z. & Zhang, H. Preparation and Applications of Mechanically Exfoliated Single-Layer and Multilayer MoS₂ and WSe₂ Nanosheets. *Accounts Chem. Res.* **47,** 1067–1075 (2014).
21. Lembke, D., Bertolazzi, S. & Kis, A. Single-Layer MoS₂ Electronics. *Accounts Chem. Res.* **48,** 100–110 (2015).
22. Tsai, D. S. *et al.* Trilayered MoS Metal SemiconductorMetal Photodetectors: Photogain and Radiation Resistance. *IEEE J. Sel. Top. Quantum Electron.* **20,** 30–35 (2014).
23. Tsai, M.-L. *et al.* Monolayer MoS₂ Heterojunction Solar Cells. *Acs Nano* **8,** 8317–8322 (2014).
24. Laskar, M. R. *et al.* Large area single crystal (0001) oriented MoS₂. *Appl. Phys. Lett.* **102,** 252108 (2013).
25. Alkis, S. *et al.* Thin film MoS₂ nanocrystal based ultraviolet photodetector. *Opt. Express* **20,** 21815 (2012).
26. Lee, Y.-H. *et al.* Synthesis of Large-Area MoS₂ Atomic Layers with Chemical Vapor Deposition. *Adv. Mater.* **24,** 2320–2325 (2012).
27. Kwak, J. Y., Hwang, J., Calderon, B., Alsalman, H. & Spencer, M. G. Long wavelength optical response of graphene-MoS₂ heterojunction. *Appl. Phys. Lett.* **108,** 091108 (2016).
28. Xue, F. *et al.* p-Type MoS₂ and n-Type ZnO Diode and Its Performance Enhancement by the Piezophototronic Effect. *Adv. Mater.* **28,** 3391–3398 (2016).
29. Li, Y., Xu, C.-Y., Wang, J.-Y. & Zhen, L. Photodiode-Like Behavior and Excellent Photoresponse of Vertical Si/Monolayer MoS₂ Heterostructures. *Sci. Reports* **4,** 7186 (2014).
30. Weiß, V., Seeger, S., Ellmer, K. & Mientus, R. Reactive magnetron sputtering of tungsten disulfide (WS₂₋ₓ) films: Influence of deposition parameters on texture, microstructure, and stoichiometry. *J. Appl. Phys.* **101,** 103502 (2007).
31. Sadale, S. B. & Patil, P. S. Synthesis of type-I textured tungsten disulfide thin films on quartz substrate. *J. Cryst. Growth* **286,** 481–486 (2006).
32. Kumar, P., Singh, M., Sharma, R. K. & Reddy, G. B. An experimental study: Role of different ambient on sulfurization of MoO₃ into MoS₂. *J. Alloys Compd.* **671,** 440–445 (2016).
33. Lee, E. W. *et al.* Growth and electrical characterization of two-dimensional layered MoS₂/SiC heterojunctions. *Appl. Phys. Lett.* **105,** 203504 (2014)
34. Mukherjee, S., Maiti, R., Katiyar, A. K., Das, S. & Ray, S. K. Novel Colloidal MoS₂ Quantum Dot Heterojunctions on Silicon Platforms for Multifunctional Optoelectronic Devices. *Sci. Reports* **6,** 29016 (2016).
35. Shaw, L. & Abbaschian, R. Chemical states of the molybdenum disilicide (MoSi₂) surface. *J. Mater. Sci.* **30,** 5272–5280 (1995).
36. Meng, Q., Zhang, J., Li, Z., Li, G. & Chen, R. Synthesis of molybdenum silicide by both ion implantation and ion beam assisted deposition. *Appl. Surf. Sci.* **254,** 2678–2684 (2008).
37. Kibsgaard, J., Chen, Z., Reinecke, B. N. & Jaramillo, T. F. Engineering the surface structure of MoS₂ to preferentially expose active edge sites for electrocatalysis. *Nat. Mater.* **11,** 963–969 (2012).
38. Jin, Z., Shin, S., Kwon, D. H., Han, S.-J. & Min, Y.-S. Novel chemical route for atomic layer deposition of MoS₂ thin film on SiO₂/Si substrate. *Nanoscale* **6,** 14453–14458 (2014).
39. Kaushik, N. *et al.* Schottky barrier heights for Au and Pd contacts to MoS₂. *Appl. Phys. Lett.* **105,** 113505 (2014).
40. Esmaeili-Rad, M. R. & Salahuddin, S. High Performance Molybdenum Disulfide Amorphous Silicon Heterojunction Photodetector. *Sci. Reports* **3** (2013).
41. Das, K., Samanta, S., Kumar, P., Narayan, K. S. & Raychaudhuri, A. K. Fabrication of Single Si Nanowire Metal SemiconductorMetal Device for Photodetection. *Ieee Trans. Electron Devices* **61,** 1444–1450 (2014).
42. Das, S., Dhyani, V., Georgiev, Y. M. & Williams, D. A. High sensitivity silicon single nanowire junctionless phototransistor. *Appl. Phys. Lett.* **108,** 063113 (2016).
43. Fontana, M. *et al.* Electron-hole transport and photovoltaic effect in gated MoS₂ Schottky junctions. *Sci. Reports* **3** (2013).

Acknowledgements

Author Contributions

V.D. conducted all the experimental works. V.D. and S.D. wrote the manuscript and assisted the interpretation of measurement data. All authors reviewed themanuscript.

Additional Information

Supplementary information accompanies this paper at http://www.nature.com/srep

Competing Interests: The authors declare no competing financial interests.

How to cite this article: Dhyani, V. and Das, S. High-Speed Scalable Silicon-MoS$_2$ P-N Heterojunction Photodetectors. *Sci. Rep.* **7**, 44243; doi: 10.1038/srep44243 (2017).

Publisher's note: Springer Nature remains neutral with regard to jurisdictional claims in published maps and institutional affiliations.